OBSERVATIONS OF GRB 041219A WITH THE SPECTROMETER ON *INTEGRAL*

S. McBreen[1], L. Hanlon[2], S. McGlynn[2], S. Foley[2], B. McBreen[2], A. von Kienlin[1], and J. French[2]

[1] *Max-Planck-Institut für extraterrestrische Physik, 85748 Garching, Germany.*
[2]*School of Physics, University College Dublin, Dublin 4, Ireland.*

ABSTRACT

GRB 041219a is the brightest burst localised by *INTEGRAL*. The peak flux of $43\,\mathrm{ph\,cm^{-2}\,s^{-1}}$ (1.84×10^{-5} $\mathrm{ergs\,cm^{-2}\,s^{-1}}$, 20 keV–8 MeV, 1 s integration) is greater than that for $\sim$98% of all bursts and the T_{90} duration of $\sim$186 s ($\sim$20 keV–8 MeV) is longer than all but a small number of bursts. The intense burst occurred about $\sim$250 s after the precursor and the long delay enabled optical and near infrared telescopes to observe the prompt emission. We present comprehensive results of the temporal and spectral analyses, including line and afterglow searches using the spectrometer, SPI, aboard *INTEGRAL*, BAT on *Swift* and ASM on *Rossi X-ray Timing Explorer*. We avail of multi-wavelength data to generate broadband spectra of GRB 041219a and afterglow. Spectra for the burst and sub–intervals were fit by the Band model and also by the quasithermal model. The high resolution Germanium spectrometer data were searched for emission and absorption features and for γ-ray afterglow.

The overall burst and sub–intervals are well fit by the Band model. The photon index below the break energy shows a marked change after the quiescent time interval. In addition the spectra are well described by a black body component with a power law. The burst was detected by BAT and ASM during the long quiescent interval in SPI indicating the central engine might not be dormant but that the emission occurs in different bands. No significant emission or absorption features were found and limits of 900 eV and 120 eV are set on the most significant features. No γ-ray afterglow was detected from the end of the prompt phase to $\sim$12 hours post-burst. Broadband spectra of the prompt emission were generated in 7 time intervals using γ-ray, x-ray, optical and near-infrared data and these were compared to the high-redshift burst GRB 050904. The optical and γ-ray emission are correlated in GRB 041219a.

Key words: Gamma ray bursts.

1. INTRODUCTION

The afterglow era of gamma–ray bursts (GRBs) has yielded many discoveries, in particular, conclusive proof of the cosmological origin and association with supernovae [e.g. 13, 29]. *INTEGRAL* has detected 37 GRBs to date [28] most of which were quite weak including a member of the low-luminosity class of bursts GRB 031203 [74, 79] and an x-ray rich burst GRB 040223 [44]. In contrast, GRB 041219a is so intense [43] that was a candidate for polarisation studies [45].

In this paper we present the results of the γ–ray spectral and temporal characteristics of the burst GRB 041219a obtained with the high resolution spectrometer, SPI, aboard *INTEGRAL* [82]. SPI is a coded-mask telescope with a fully coded field of view of 16° that uses a 19 pixel high spectral resolution Ge detector. The detectors cover the energy range 20 keV–8 MeV with an energy resolution of 2-8 keV FWHM. A detailed description of SPI can be found in Vedrenne et al (2003) [77]. Analysis of the light curves observed by Burst Alert Telescope (BAT) on *Swift* in the range 15 –350 keV [22] and the Rossi X-ray Timing Explorer All Sky Monitor (ASM) in the energy range 1.5–12 keV [38] are also presented. GRB 041219a is the brightest burst detected by the *INTEGRAL* burst alert system (IBAS) [46] and prompt emission was detected in the optical [78] and near infrared [6].

2. OBSERVATIONS

GRB 041219a was detected by IBAS at 01:42:18 UTC on December 19^{th} 2004 [27] at a location of right ascension 00h 24m 25.8s, declination $+62^{\circ}\ 50'\ 05.6''$ (Galactic latitude and longitude of 0.12°, 119.85°) at a detector off-axis angle of 3.2°. GRB 041219a was also detected by BAT [5] at a location consistent with the IBAS position. Levine & Remillard (2004) [37] reported a serendipitous observation of GRB 041219a during two 90 s dwell times with the *Rossi X-ray Timing Explorer* All Sky Monitor (ASM) in the energy range 1.5–12 keV [38]. The burst was in the field of view from 6 s after the trigger for 3 minutes apart from a 6 s gap. Prompt optical emission correlated with the γ-ray emission was reported Vestrand et al. [78]. Infrared emission was detected 7.2 minutes after the burst trigger at the tail end of the prompt γ-ray emission [6]. There is no measured redshift available for this burst.

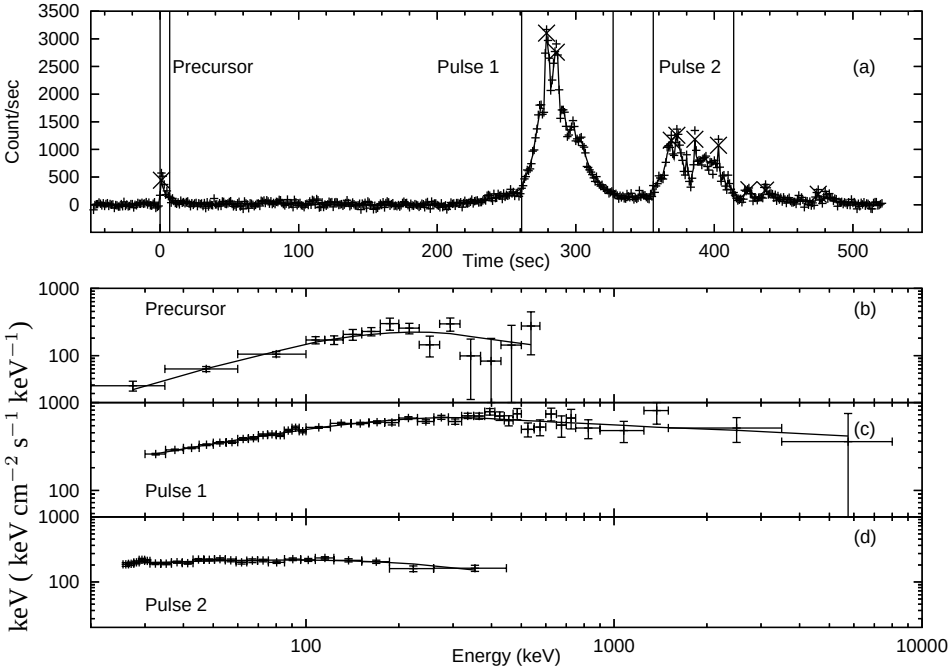

Figure 1. SPI light curves and spectra of GRB 041219a. (a) denoised and background subtracted light curve where significant pulses selected by the algorithm are marked with an x. The three marked sections denote the time intervals over which the spectra were analysed. The start and end times of the intervals and the parameters of best fit Band spectra are presented in Table 1. Spectrum and Band model fits for (b) the precursor pulse (0–7 s); (c) pulse 1 (261–327 s); (d) pulse 2 (356–414 s).

3. ANALYSIS AND RESULTS

3.1. Light Curves

The SPI light curve in the broad energy band from 20 keV – 8 MeV at 1 s resolution is given in Fig. 1 (a). The light curves are generated from housekeeping data [51]. A section of the light curve detected by the BAT is shown in Fig. 2 using the data from Fenimore et al. (2004) [20] and no spectral information is available. The T_{90} value of 186 s ($\sim$20 keV–8 MeV) was determined from the SPI light curve. T_{90} is the time for 5 to 95% of the flux to be accumulated and the values are shorter than the burst duration in this case because of the quiescent interval and the precursor has only $\sim$2% of the counts. The temporal structure of the burst is unusual, with an initial weak precursor pulse followed by a long quiescent time interval and the main emission beginning at $\sim$ 250 s post–trigger (Fig. 1 (a)). The SPI light curve was denoised using a wavelet analysis [64] and the pulses selected by a pulse decomposition algorithm are shown in Fig. 1 (a). Although the SPI light curve is quiescent from $\sim$7–200 s, emission is detected in the BAT light curve particularly in the lower energy channels 1 and 2 (Fig. 2) (15-25 keV and 25- 50 keV) [20]. In addition a spectrally soft pulse was detected in the ASM [37] beginning at 80 s in the quiescent period of the SPI observation (Fig. 2). The value of T_{90} depends very much on the bandwidth over which it is measured.

3.2. Spectral Analysis

The spectrum of GRB 041219a was extracted using Online Software Analysis version 5.0 available from the *INTEGRAL Data Science Centre* [1]. GRB 041219a is the brightest burst localised by *INTEGRAL* to date. Its peak flux of 43 ph cm^{-2} s^{-1} (1.84×10^{-5} ergs cm^{-2} s^{-1}) (20 keV–8 MeV, 1 s integration) is greater than $\sim$98% of bursts detected by BATSE while its T_{90} duration of 186 s ($\sim$20 keV–8 MeV) is longer than all but a handful ($\sim$4%) of BATSE GRBs [56]. The spectrum of the burst and sub-intervals are well fit by the Band model [2] and the parameters are presented in Fig. 1 and Table 1 (Columns 1–8). The parameters of the spectrum evolve during the burst. For instance α is remarkably higher in the initial pulse in comparison to the main emission phase. The peak energy, E_{peak}, is given by $(2+\alpha)\times E_0$ and the evolution of E_{peak} shows softening in the main emission phase.

Ryde (2005) [72] suggested that thermal emission may be ubiquitous in GRBs and fit a black body + power law model to a number of bright BATSE bursts. Ryde (2005) [72] reported that the temperature was intially constant or weakly decreasing with a shallow power law and that the power law index steepened throughout the burst. We fit the quasithermal model to GRB 041219a and the results are shown in Table 2 and Fig. 3. In this interpretation the black body contributes more strongly in the precursor

[1] http://isdc.unige.ch/

Table 1. Spectral properties of GRB 041219a. The columns refer to the emission region, time interval of spectral fits, low-energy power-law index (α), high-energy power-law index (β), break energy (E_0), χ^2/degrees of freedom (dof) of the fit, fluence in the range 20–200 keV ($S_{20-200\ \mathrm{keV}}$) and fluence in the range 20 keV–8 MeV ($S_{20\ \mathrm{keV}-8\ \mathrm{MeV}}$). Errors on spectral parameters quoted for a 90% confidence level and the fit parameters are for the spectra shown in Fig. 1.

Emission Region	Time (s)	α	β	E_0 (keV)	χ^2/*dof*	$S_{20-200\ \mathrm{keV}}$ (erg cm^{-2})	$S_{20\ \mathrm{keV}-8\ \mathrm{MeV}}$ (erg cm^{-2})
Precursor	0–7	$-0.45\ ^{+0.37}_{-0.30}$	$-2.62\ ^{+0.73}_{-7.4}$	$145.4\ ^{+79.7}_{-48.1}$	12.1/11	2.8×10^{-6}	7.1×10^{-6}
1st Pulse	261–327	$-1.5^{+0.08}_{-0.06}$	$-1.95\ ^{+0.08}_{-0.21}$	$568.3\ ^{+310}_{-205.2}$	57.5/50	7.0×10^{-5}	2.6×10^{-4}
2nd Pulse	356–414	$-1.76\ ^{+0.09}_{-0.08}$	$-3^{\dagger}$	$363.6\ ^{+193.1}_{-99.5}$	30.9/21	4.0×10^{-5}	1.0×10^{-4}
1st & 2nd Pulse	261–414	$-1.43\ ^{+0.08}_{-0.06}$	$-2.06\ ^{+0.09}_{-0.12}$	$299.2\ ^{+76.2}_{-73.9}$	16.5/25	1.3×10^{-4}	3.7×10^{-4}
Burst	0–580	$-1.48\ ^{+0.08}_{-0.07}$	$-1.92\ ^{+0.07}_{-0.13}$	$365.9\ ^{+191.6}_{-108.2}$	51.9/30	1.6×10^{-4}	5.7×10^{-4}

† β value frozen at -3.

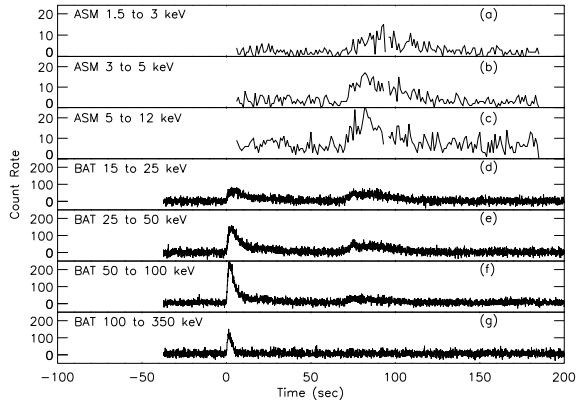

Figure 2. Rossi ASM (a-c) and Swift BAT (d-g) light curves of GRB 041219a up to $T_0 + 200$ s. Rossi ASM data are available only for two 90 s dwell times starting at $T_0 + 6$ s and $T_0 + 96$ s. The ASM and BAT light curves have emission in the interval at about 80 s that is quiescent in the SPI light curve (Fig. 1). The Rossi-ASM data were obtained courtesy of Alan Levine.

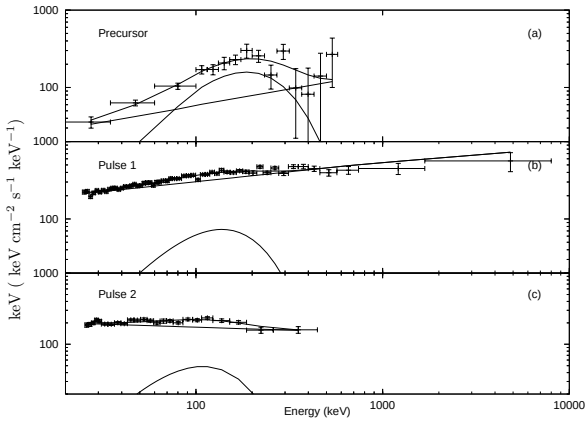

Figure 3. Spectral fits to (a) the precursor, (b) pulse 1 and (c) pulse 2 of GRB 041219a using combined black body and power law fits. The data are shown along with the combined fit and the black body and power law components.

than in pulses 1 and 2.

3.3. Spectral lines

A search for line emission in the SPI data was carried out on the brightest pulse in the burst. The search involved finding the best continuum model for the data and then adding a gaussian emission line of varying width (1 keV to 20 keV) to the model at energies from 30 keV to 1 MeV. The F-test was used to evaluate the resulting improvement in the fit for each line width and each energy. However, it is well known that the F-test alone cannot be used to check for the presence of a line [63] and must be calibrated for false positives. The spectrum for which the largest F-test value was obtained was chosen and Monte Carlo simulations were carried out to test the number of times a more significant F-test value would be detected in simulated data of the continuum model. A large number of spectra (10,000) of the continuum were generated. The Band model and Band model+ emission line were fit to each generated spectrum and the F-test for the improvement in the fit was recorded for each. The same approach was adopted to search for absorption features. The false positive rate was evaluated.

The most significant emission line feature was 4 keV wide at 89 keV with an F-test value of 4.6. Of the 10,000 simulated spectra, 5850 resulted in an improvement in χ^2 and out of this fraction 5.2% of trials resulted in a higher value of F-test than 4.6. The equivalent width of this emission line is 900 eV (1.4×10^{-9} ergs). The most significant absorption feature had a width of 3 keV at 103 keV with an F-test value of 7.8. Of the 10,000 simulations that were run, 5876 resulted in an improvement in χ^2 and 2.5% of these produced an F-test value higher than 7.8. The equivalent width of this absorption feature is 120 eV (1.9×10^{-10} ergs). No significant emission or absorption features were found.

Table 2. Spectral fits to GRB 041219a using the quasithermal model. The columns refer to the emission region, time interval of spectral fits, kT, power-law index (Γ), χ^2/degrees of freedom (dof) of the fit. Errors on spectral parameters quoted for a 90% confidence level.

Emission Region	Time (s)	*kT*	Γ	χ^2/*dof*	$S_{20-200\ keV}$ in the blackbody component (ergs cm^{-2} s^{-1})	% Flux in the blackbody component (20-200 keV)
Precursor	0–7	$45.7^{+9.1}_{-8.7}$	$1.58^{+0.53}_{-0.28}$	9.25/11	1.4×10^{-6}	49%
1$^{\rm st}$ Pulse	261–327	$35.1^{+5.5}_{-4.7}$	$1.74^{+0.02}_{-0.02}$	68/50	8.7×10^{-6}	11.6%
2$^{\rm nd}$ Pulse	356–414	$27.3^{+4.9}_{-4.8}$	$2.1^{+0.70}_{-0.08}$	28.9/21	5.8×10^{-6}	12.7%

3.4. Afterglow Search with SPI

A search for a γ–ray afterglow was performed on the available data for up to 12 hours after the burst trigger. The data was split into three separate time intervals and a spectrum extracted. Significant emission from the burst position was not detected even when the data were summed over the entire 12 hours. The 3 σ upper limits for the subsequent time intervals are given in Fig. 4.

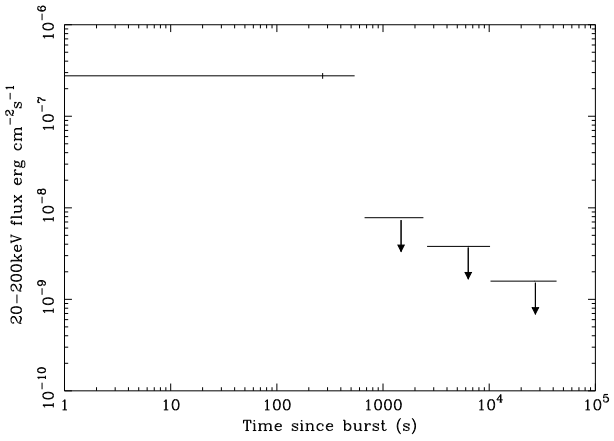

Figure 4. The flux averaged over the burst duration of GRB 041219a and 3 σ upper limits in the energy range 20–200 keV. The arrows give the 3 σ limits over the time 670 s to 43000 s after the burst.

3.5. Broadband spectra

The broadband spectra of the prompt emission for the GRB 041219a are plotted in 7 time intervals using a combination of γ-ray data from SPI and BAT, x-ray data from ASM, optical data from Vestrand et al. (2005) [78] and infrared data from Blake et al (2005) [6] corrected for extinction. Fig. 5 shows three spectra during the initial $\sim$120 s generated from *Rossi*-ASM, *Swift*-BAT and *INTEGRAL*-SPI data in three different time intervals. The broadband spectra of the prompt emission for GRB 041219a are given in Fig. 6 for the four time intervals of simultaneous optical and gamma observations. In the case of the interval (D) there are also simultaneous near infrared results from PARITEL [6]. The broadband spectra of GRB 041219a were originally presented by Vestrand et al. (2005) [78] . The energy range has been expanded here by including the SPI results for intervals (A) to (D) and near infrared results for interval (D). The broadband spectrum of the afterglow from GRB 041219a is shown 12 hours after the burst (E) using infrared and optical data from Blake et al (2005) [6] and Sonoda et al. (2004) [75] respectively and an upper limit from SPI. The simultaneous optical, x-ray [7] and gamma ray results for the high redshift GRB 050904 are shown in the interval 151 to 254 s for comparison.

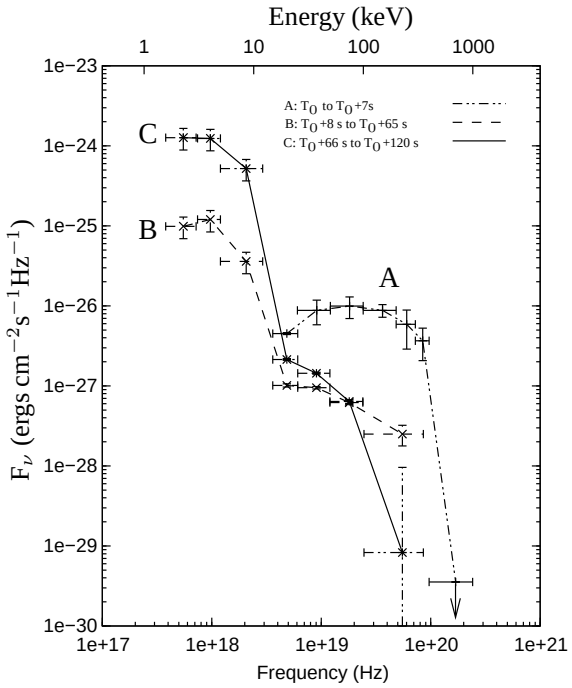

Figure 5. Broadband spectra of the initial 120 s of GRB 041219a in the x-ray and gamma ray region. The data are plotted in flux density (ergs cm^{-2} s^{-1}Hz^{-1}) versus observed frequency (lower axis) and keV (upper axis). The first interval (T_0 to T_0+7 s) includes the precursor pulse and the third interval T_0+66 s to T_0+120 s includes the soft pulse in the long quiescent interval. The broad spectra were generated using ASM x-ray data and γ-ray data from BAT and SPI.

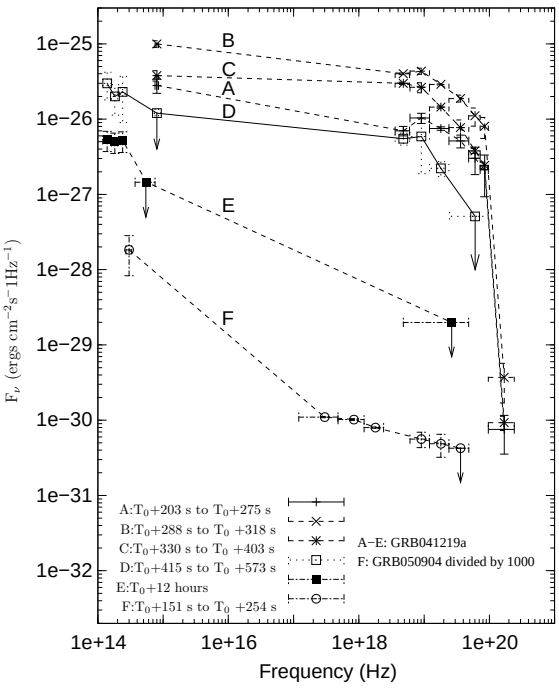

Figure 6. Broadband spectra of GRB 041219a (A to E) and GRB 050904 (F). The four intervals (A to D) are defined by the periods of simultaneous RAPTOR optical observations of GRB 041219a [78]. The RAPTOR optical results are shown and connected by a line to the lowest energy BAT channel and the higher energy SPI channels. The PARITEL near infrared results [6] are shown for interval D and connect by a solid line with the optical upper limit and the γ-ray data. The broadband spectrum of the afterglow from GRB 041219a is shown 12 hours after the burst (E) combining data from Blake et al. [6], Sonoda et al. [75] and SPI. The simultaneous optical, x-ray [7] and γ-ray results for GRB 050904 are shown for the interval 151 to 254 s and have been divided by 10^3 for clarity.

4. DISCUSSION

4.1. Spectral behaviour of GRB 041219a

In most GRB models, the main event is preceded by less intense emission, characterised by a thermal spectrum, called a precursor. Precursors are associated with the transition of the fireball from an optically thick to an optically thin environment [e.g. 59, 65]. A rigorous definition of precursors is problematic because of the complexity of GRB temporal structures. Koshut et al (1995) [35] defined precursors that had a peak intensity lower than that of the whole burst and were followed by a period of quiescence longer than the remaining duration of the burst. Soft precursors, occurring before the trigger, have been detected by many instruments e.g. *Ginga* [53]. The *Ginga* precursor has a thermal spectrum and has been compared with theoretical expectations [65]. The precursor pulse was fit by a Band model and a black blody+power law model and is quite different from the main emission. The properties of the precursor spectrum are shown in Tables 1 and 2 respectively.

The β values for a simple cooling spectrum and an instantaneous spectrum, in which cooling effects are negligible, are $-\frac{(p+2)}{2}$ and $-\frac{(p+1)}{2}$ respectively, where p is the electron index. From Table 1, using the well constrained β values for the main emission phase, the derived p values are $2.12^{+0.24}_{-0.18}$ and $3.12^{+0.18}_{-0.24}$.

The value of α changes significantly between the precursor and main emission phase. α is predicted by the synchrotron shock model to be between $-3/2$ and $-1/2$, although taking into account non-isotropic electron pitch angles and/or self-absorption can produce α values up to and above 0 [39]. The evolution of α may be evidence of changes in opacity or electron pitch angle from pulse to pulse. There is a tendency for low break energies to give harder α values, since the spectrum does not reach the asymptotic value in the limited spectral fitting window. The majority of GRBs have low energy power law spectral indices in the range $-3/2 < \alpha < -2/3$ [e.g. 14, 61, 23]. However a substantial fraction of GRBs have $\alpha > -2/3$ and lie outside the optically thin synchrotron model [60].

A number of authors have discussed the possibility of fitting thermal components to time resolved or average GRB spectra [e.g. 24, 32, 71, 72, 8]. Ghirlanda et al. (2003) [24] studied time resolved spectra of a number of BATSE bursts with very hard spectra and found that the spectra were not adequately explained by non-thermal emission models. In fact, they found that spectra early in the burst were well fit by a black body spectral model. We find an improvement in χ^2 for the blackbody+power law model over the Band model for the precursor phase of GRB 041219a where 49% of the flux is contained in the blackbody component (Table 2). The Band model provides a better description of the continuum spectrum in pulse 1 and similar goodness of fit values are achieved for pulse 2. The fits of the quasithermal model show that the value of *kT* is highest for the precursor pulse and declines during the burst. Recently, Ryde (2005) [72] studied the prompt emission from a sample of the bright pulses in the catalogue and found that time resolved spectra were equally well fitted by the black body+power law model and with the Band model. The spectrum of GRB 041219a can also be described by the quasithermal model (Table 2). Recently, Rees & Mészáros(2005) [68] suggested that the $E_{\rm peak}$ in the γ-ray spectrum is due to the Comptonized thermal component from the photosphere, where the comoving optical depth falls to unity. The thermal emission from a laminar and steady jet when viewed head-on, would give rise to a thermal spectrum peaking in the x-ray or γ-ray band. The resulting spectrum would be the superposition of the Comptonized thermal component and the power law from the synchrotron emission.

4.2. Spectral lines

The issue of narrow spectral lines in the prompt emission from GRBs has been controversial. The line features originally identified in spectra at $\sim 20-60$ keV [40] were interpreted as cyclotron line emission from electrons in neutron star magnetic fields and were used to support the neutron star origin hypothesis for GRBs. The BATSE Spectroscopy Detectors were determined to be quite capable of detecting features [3], such as had been reported by *Ginga* [52], if they were a common occurance. The results from an automated line search of BATSE data, however, were inconclusive [9]. No strong evidence for γ-ray emission or absorption features has been found in the brightest pulse of GRB 041219a.

4.3. Temporal behaviour GRB 041219a

GRB 041219a has an unusual time history because the initial pulse is followed by a long period of quiescence. However it should be noted that although the time interval is quiescent in the SPI light curve, emission is detected in the three *Rossi*-ASM and *Swift*-BAT light curves (Fig. 2) at $\sim$T$_0$+80 s. Similar light curves with a weak triggering pulse followed by a long quiescent time interval have been observed by BATSE [21]. The sample of Quilligan et al (2002) [64] contained 319 bright BATSE GRBs and two of the bursts show similar temporal evolution to GRB 041219a (triggers 6451 and 7575). In addition the γ-ray light curves of GRB 050820a [57, 11] and GRB 060124 [30, 69] show a similar weak precursor pulse and a long quiescent interval before the main pulse as noted by Pal'Shin & Frederiks (2005) [58] and Golenetskii et al. (2006) [26].

Lazzati (2005) [36] searched for 'non-triggering' precursors in a sample of bright, long BATSE burst light curves and found that in 20% of cases there is evidence of emission above the background coming from the same direction as the GRB. This emission is characterized by a softer spectrum with respect to the burst spectrum and contains up to 1% of the counts and typically has a non-thermal power-law spectrum. The precursor type pulse in GRB 041219a contains 2% of the total fluence (50–300 keV) and is similar to precursors in the BATSE sample, except that it was a triggering event. A number of studies have been made of periods of quiescence in GRBs. A trend was found between the duration of the quiescent time and duration of the following emission period [66] that is consistent with GRB 041219a. Quilligan et al (2002) [64] showed that the measured distribution of time intervals between pulses in BATSE bursts is best fit by lognormal with allowance made for the excess in time intervals > 15 s. The Pareto Lévy tail [50] of the time intervals is well fit by a power-law of slope ~ -1 [64].

The model of a GRB as a relaxation system [41], which continuously accumulates energy and discontinuously releases it accounts for the correlated pulses properties and time intervals between pulses [42, 54]. This model can be extended to include periods of quiescence if the system returns to a more stable configuration that might be caused by a total release of accumulated energy. These general considerations do not identify the emission mechanism. Periods of quiescence can in principle, be caused by a modulated relativistic wind or a switching off of the central engine [67]. Drago & Pagliara (2005) [17] found that similarities between the pre- and post-emission periods suggest that both emission periods are produced by the same mechanism and that long quiescent intervals are generated by a switching off of the engine rather than a modulation of a continuous wind. However, it should be noted that GRB 041219a was detected at lower energies by BAT and ASM during the long quiescent interval in SPI indicating the central engine might not be dormant but that the emission occurs in different bands.

4.4. Broadband spectra

The broadband spectra of the precursor pulse and the weak pulse at $\sim$60 s in the long quiescent interval are given in Fig. 4. The ASM observations (Fig. 2) start at the end of the precursor pulse. The BAT and SPI data show that the spectrum of the precursor peaked at about 2×10^{19} Hz ($\sim$83 keV) and is quite different from the broadband spectra in the two subsequent intervals from 8 to 65 s and 66 to 120 s where there is strong emission in the x-ray band. The dominance of the emission in the x-ray band is apparent in the ASM and BAT profiles in Fig. 2.

In contrast the broadband spectra over the four intervals (A to D in Fig 6) are remarkably similar because the simultaneous optical emission is correlated with the gamma ray burst. This correlation would arise naturally if the emission in both bands were generated by a common mechanism. The most likely mechanism is that the optical emission is the low energy tail of the synchrotron radiation generated by internal shocks in the outflow [e.g. 33, 47]. Fan et al. (2004) [19] and Fan et al. (2005) [18] have suggested that the optical/near IR flash could be the result of emission from neutron-rich internal shocks colliding at a larger distance from the central engine. There are simultaneous J, H and K infrared observations in interval D that are an extrapolation of the optical data. The J, H and K-band observations 12 hours after the burst (E in Fig. 6) are similar but less intense and mark the transition from the burst to the afterglow. This similarity between the two measurements indicate that the infrared emission is due to the afterglow and it was already well developed in interval D and has been well modelled as the superposition of a reverse shock and a forward shock component [19].

There is an interesting contrast between the broadband spectra of GRB 041219a and GRB 050904 (F in Fig. 6) because of the large difference between the simultaneous optical and γ-ray emission in the two bursts. The five GRBs that have been detected as strong optical sources during the prompt γ-ray emission are GRB 990123 at

z = 1.60 [1], GRB 041219a with no spectroscopic redshift, GRB 050401 at $z = 2.9$ [73], GRB 050904 at $z = 6.29$ [7, 80, 76, 16, 81] and GRB 0601111b with no spectroscopic redshift [34]. The flux densities at the maximum of the optical emission are respectively 1080 mJy (V-band), 3.1 mJy (R-band), 2.6 mJy (R-band), 1300 mJy (V-band) and $\sim$360 mJy (clear filter) if it is assumed that all GRBs are at the same redshift of 1.6 for GRB 990123 [7]. At $z = 1.6$ the optical emission from GRB 990123, GRB 050904 and GRB 0601111b are comparable and exceed that from GRB 041219a and GRB 050401 by a factor of several hundred. The bright optical emission from GRB 990123, GRB 050904 and GRB 0601111b has been attributed to the reverse shock. This powerful emission is not dominant in GRB 041219a and GRB 050401 because it would have overwhelmed the observed emission. Furthermore the strong optical emission from the reverse shock is not a common feature of most GRBs [70]. In the additional case of GRB 060124 at a redshift of 2.297 [48, 12, 62] recent simultaneous optical and γ-ray observations with *Swift* reveal prompt optical emission with a peak of 16.88 magnitude in the V-Band (0.55mJy) [31]. The UVOT instrument was in image mode at early times and high time resolution data was not available. Romano et al. (2006) [69] rule out a reverse shock based on the level of the optical emission and furthermore, since the optical data do not clearly track the γ-ray emission, they suggest that external shocks may be the source of the optical emission. The long duration and nearby (z=0.0331 [49]) weak burst/x-ray flash GRB 060218/SN 2006aj has simultaneous optical and γ-ray observations with *Swift* [15, 10]. The peak of the prompt optical emission is only 0.118 mJy in the V band [10] and is smaller than the bright optical emission from GRB 990123 by a factor of $\sim 10^8$ (if both bursts were at a redshift of z=1.6) yielding a much larger ratio in prompt optical than in the prompt γ-ray emission.

These results underline the need for continued broadband observations of the prompt emission phase and the early afterglow.

ACKNOWLEDGMENTS

SMB acknowledges the support of the European Union through a Marie Curie Intra-European Fellowship within the Sixth Framework Program.

REFERENCES

[1] Akerlof, C., Balsano, R., Barthelemy, S., et al. 1999, Nature, 398, 400

[2] Band, D., Matteson, J., Ford, L., et al. 1993, ApJ, 413, 281

[3] Band, D. L., Ford, L. A., Matteson, J. L., et al. 1995, ApJ, 447, 289

[4] Barkov, M. V. & Bisnovatyi-Kogan, G. S. 2005, [astro-ph/0503414]

[5] Barthelmy, S., Burrows, D., Cummings, J., et al. 2004, GCN 2874

[6] Blake, C. H., Bloom, J. S., Starr, D. L., et al. 2005, Nature, 435, 181

[7] Boër, M., Atteia, J. L., Damerdji, Y., et al. 2006, ApJL, 638, L71

[8] Bosnjak, Z., Celotti, A., & Ghirlanda, G. 2006, [astro-ph/0604425]

[9] Briggs, M. S., Pendleton, G. N., Brainerd, J. J., et al. 1998, in American Institute of Physics Conference Series, ed. C. A. Meegan, R. D. Preece, & T. M. Koshut, 104

[10] Campana, S., Mangano, V., Blustin, A. J., Brown, P., & Burrows, D. N. 2006, [astro-ph/0603279]

[11] Cenko, S. B., Kasliwal, M., & Harrison, F. 2006, astro-ph/0608183

[12] Cenko, S. B., Berger, E., & Cohen, J. 2006, GRB Coordinates Network, 4592, 1

[13] Costa, E., Frontera, F., Heise, J., et al. 1997, Nature, 387, 783

[14] Crider, A., Liang, E. P., Smith, I. A., et al. 1997, ApJL, 479, L39

[15] Cusumano, G., Barthelmy, S., Gehrels, N., et al. 2006, GRB Coordinates Network, 4775, 1

[16] Cusumano, G., Mangano, V., Chincarini, G., et al. 2005, [astro-ph/0509737]

[17] Drago, A. & Pagliara, G. 2005, [astro-ph/0512602]

[18] Fan, Y. Z. & Wei, D. M. 2004, ApJL, 615, L69

[19] Fan, Y. Z., Zhang, B., & Wei, D. M. 2005, ApJL, 628, L25

[20] Fenimore, E., Barthelmy, S., Cummings, J., et al. 2004, GCN 2906

[21] Fishman, G. J., Meegan, C. A., Wilson, R. B., et al. 1994, ApJSS, 92, 229

[22] Gehrels, N., Chincarini, G., Giommi, P., et al. 2004, ApJ, 611, 1005

[23] Ghirlanda, G., Celotti, A., & Ghisellini, G. 2002, A&A, 393, 409

[24] Ghirlanda, G., Celotti, A., & Ghisellini, G. 2003, A&A, 406, 879

[25] Ghirlanda, G., Ghisellini, G., & Lazzati, D. 2004, ApJ, 616, 331

[26] Golenetskii, S., Aptekar, R., Mazets, E., et al. 2006, GRB Coordinates Network, 4599,

[27] Götz, D., Mereghetti, S., Shaw, S., et al. 2004, GCN 2866

[28] Hanlon, L., Foley, S., McBreen, S., et al 2007, this proceedings

[29] Hjorth, J., Sollerman, J., Møller, P., et al. 2003, Nature, 423, 847

[30] Holland, S. T., Barthelmy, S., Burrows, D. N., et al. 2006, GRB Coordinates Network, 4570

[31] Holland, S. T., Smith, P., Huckle, H., & Gehrels, N. 2006, GRB Coordinates Network, 4580

[32] Kaneko, Y., Preece, R. D., & Briggs, M. S. 2003, American Astronomical Society Meeting Abstracts, 203

[33] Katz, J. I. 1994, ApJL, 432, L107

[34] Klotz, A., Gentre, B., Stratta, G., et al. 2006, [astro-ph/0604061]

[35] Koshut, T. M., Kouveliotou, C., Paciesas, W. S., et al. 1995, ApJ, 452, 145

[36] Lazzati, D. 2005, MNRAS, 357, 722

[37] Levine, A. & Remillard, R. 2004, GRB Coordinates Network, 2917,

[38] Levine, A. M., Bradt, H., Cui, W., et al. 1996, ApJL, 469, L33

[39] Lloyd, N. M. & Petrosian, V. 2000, ApJ, 543, 722

[40] Mazets, E. P., Golenetskii, S. V., Aptekar, R. L., Guryan, Y. A., & Ilinskii, V. N. 1980, Soviet Astronomy Letters, 6, 372

[41] McBreen, S., McBreen, B., Hanlon, L., & Quilligan, F. 2002, A&A, 393, L29

[42] McBreen, S., McBreen, B., Quilligan, F., & Hanlon, L. 2002, A&A, 385, L19

[43] McBreen, S., Hanlon, L., McGlynn, S., & et al., 2006, A&A, 455, 433

[44] McGlynn, S., McBreen, S., Hanlon, L., et al. 2005, Il Nuovo Cimento C, vol. 28, Issue 4, p.481

[45] McGlynn, S., Clark, D. K., Dean, A. J., Hanlon, L., et al. 2007, A&A accepted, [astro-ph/0702738]

[46] Mereghetti, S., Götz, D., Borkowski, J., Walter, R., & Pedersen, H. 2003, A&A, 411, L291

[47] Mészáros, P. & Rees, M. J. 1999, MNRAS, 306, L39

[48] Mirabal, N. & Halpern, J. P. 2006, GRB Coordinates Network, 4591,

[49] Mirabal, N. & Halpern, J. P. 2006, GRB Coordinates Network, 4792,

[50] Montroll, E. W. & Shlesinger, M. F. 1982, Proceedings of the National Academy of Sciences of the United States of America-Physical Sciences, 79, 3380

[51] Moran, L., Mereghetti, S., Götz, D., et al. 2005, A&A, 432, 467

[52] Murakami, T., Fujii, M., Hayashida, K., Itoh, M., & Nishimura, J. 1988, Nature, 335, 234

[53] Murakami, T., Inoue, H., Nishimura, J., van Paradijs, J., & Fenimore, E. E. 1991, Nature, 350, 592

[54] Nakar, E. & Piran, T. 2002, ApJL, 572, L139

[55] Norris, J. P., Marani, G. F., & Bonnell, J. T. 2000, ApJ, 534, 248

[56] Paciesas, W. S., Meegan, C. A., Pendleton, G. N., et al. 1999, ApJS, 122, 465

[57] Page, M., Burrows, D., Beardmore, A., et al. 2005, GRB Coordinates Network, 3830,

[58] Pal'Shin, V. & Frederiks, D. 2005, GRB Coordinates Network, 3852,

[59] Piran, T. 2004, Reviews of Modern Physics, 76, 1143

[60] Preece, R. D., Briggs, M. S., Giblin, T. W., et al. 2002, ApJ, 581, 1248

[61] Preece, R. D., Briggs, M. S., Mallozzi, R., et al. 2000, ApJS, 126, 19

[62] Prochaska, J. X., Foley, R., Tran, H., Bloom, J. S., & Chen, H.-W. 2006, GRB Coordinates Network, 4593,

[63] Protassov, R., van Dyk, D. A., Connors, A., Kashyap, V. L., & Siemiginowska, A. 2002, ApJ, 571, 545

[64] Quilligan, F., McBreen, B., Hanlon, L., et al. 2002, A&A, 385, 377

[65] Ramirez-Ruiz, E., MacFadyen, A. I., & Lazzati, D. 2002, MNRAS, 331, 197

[66] Ramirez-Ruiz, E. & Merloni, A. 2001, MNRAS, 320, L25

[67] Ramirez-Ruiz, E., Merloni, A., & Rees, M. J. 2001, MNRAS, 324, 1147

[68] Rees, M. J. & Mészáros, P. 2005, ApJ, 628, 847

[69] Romano, P., Campana, S., Chincarini, G., et al. 2006, [astro-ph/0602497]

[70] Roming, P. W. A., Schady, P., Fox, D. B., et al. 2005, [astro-ph/0509273]

[71] Ryde, F. 2004, ApJ, 614, 827

[72] Ryde, F. 2005, ApJL, 625, L95

[73] Rykoff, E. S., Yost, S. A., Krimm, H. A., et al. 2005, ApJL, 631, L121

[74] Sazonov, S. Y., Lutovinov, A. A., & Sunyaev, R. A. 2004, Nature, 430, 646

[75] Sonoda, E., Maeno, S., Matsuo, Y., & Yamauchi, M. 2004, GRB Coordinates Network, 2882

[76] Tagliaferri, G., Antonelli, L. A., Chincarini, G., et al. 2005, A&A, 443, L1

[77] Vedrenne, G., Roques, J. P., Schönfelder, V., et al. 2003, A&A, 411, L63

[78] Vestrand, W. T., Wozniak, P. R., Wren, J. A., et al. 2005, Nature, 435, 178

[79] Watson, D., Hjorth, J., Levan, A., et al. 2004, ApJl, 605, L101

[80] Watson, D., Reeves, J. N., Hjorth, J., et al. 2006, ApJL, 637, L69

[81] Wei, D. M., Yan, T., & Fan, Y. 2005, [astro-ph/0511154]

[82] Winkler, C., Courvoisier, T. J. L., Di Cocco, G., et al. 2003, A&A, 411, L1